Electronic Supplementary Information

Unraveling the reactions between a hydride-protected Ag_{18} nanocluster and thiol by the crystallization of intermediates

Subrata Duary, [a] Samapti Mondal, [a] Souvik Manna,[b] Soham Chowdhury, [a] Biswarup Pathak*[b] and Thalappil Pradeep*[a]

[a] *DST Unit of Nanoscience (DST UNS) and Thematic Unit of Excellence (TUE), Department of Chemistry, Indian Institute of Technology Madras, Chennai–600036, India.*

**E-mail: pradeep@iitm.ac.in*

[b] *Department of Chemistry, Indian Institute of Technology Indore, Indore 453552, India.*

**E-mail: biswarup@iiti.ac.in*

Materials and chemicals

Silver nitrate ($AgNO_3$) was purchased from Rankem Chemicals. Triphenyl phosphine and sodium borohydride ($NaBH_4$, 98%) were bought from Aldrich. 2,3,5,6-Tetrafluoro-4-(trifluoromethyl)benzenethiol was purchased from Tokyo Chemical Industry (India) Pvt. Ltd. Milli-Q water was used for $[Ag_{18}H_{16}(TPP)_{10}]^{2+}$ synthesis and its purification. HPLC-grade solvents such as methanol, chloroform, and acetone were purchased from Rankem chemicals. All the chemicals are commercially available and used as such without any purification.

Experimental section

Synthesis of $[Ag_{18}H_{16}(TPP)_{10}]^{2+}$

The $[Ag_{18}H_{16}(TPP)_{10}]$ nanocluster was synthesized by following a reported synthesis procedure.[1] In brief, 20 mg $AgNO_3$ was dissolved in 5 mL methanol, and 5 mL chloroform was added to it in a bottle, stirred at 700 rpm and room temperature. Next, 65 mg triphenyl phosphine dissolved in 4 mL of chloroform was added to it. It was allowed to be stirred for 15 minutes. After that, 6.5 mg sodium borohydride dissolved in 1 mL ice-cold water was added to it, and immediately the colour of solution turns to transparent yellowish from colourless solution. The reaction was continued on stirring for 3.5 h in dark condition. Gradually, the colour of solution changes to brownish black and finally dark green, which indicates the formation of the nanocluster. Then, the mixed solvent was evaporated under reduced pressure in rotavapor, and the solid green product was repeatedly washed to remove excess reagent. The cluster is soluble in methanol and characterized using UV-vis. and mass spectrometry. The purified cluster was extracted in methanol, and used for further study. The yield of the product was 35% in terms of silver.

Ligand exchange with 2, 3, 5, 6-tetrafluoro-4-(trifluoromethyl) benzene thiol

Cleaned Ag_{18} nanocluster was reacted with thiol (2,3,5,6-Tetrafluoro-4-(trifluoromethyl)benzenethiol) at different molar ratios (cluster : thiol, 1:1, 1:2 and 2:1 respectively). For 1:1 ratio, the Ag-1 was crystallized directly from crude mixture after 5 min stirring by hexane diffusion into it at 4 °C, and Ag-6 was crystallized in a MeOH-$CHCl_3$ (1:1) mixture from reaction mixture after 45 min.

Characterization techniques

Absorption spectra of cluster in solution was recorded using a Perkin Elmer Lambda 365 UV-vis spectrometer with a band pass filter of 1 nm. Mass of nanoclusters (NCs) was measured in a Waters SynaptG2Si high-definition mass spectrometer. The following conditions-flow rate10 µL/min, a capillary voltage of 2.50 kV, a source temperature of 100 °C, desolvation temperature of 150 °C with a desolvation rate of 400 L/h, and trap gas 2 mL/min were applied for ionization of the NCs. The photoluminescence (PL) spectra was recorded using Jobin Yvon Nanolog fluorescence spectrometer with a band pass of 3 nm for excitation and emission. X-ray photoelectron spectroscopy (XPS) of NCs was recorded using an ESCA Probe TPD spectrometer of Omicron Nanotechnology, equipped with a polychromatic Mg Kα X-ray source (hν =1253.6 eV). The binding energy of different elements was calibrated for C 1s (285.0 eV). Single crystal X-ray diffraction (SC-XRD) data of single crystals were collected using a Bruker D8 VENTURE instrument, equipped with a Mo Kα radiation source (0.71 Å) and a PHOTON 100 CMOS detector. The structure was solved by SHELXT-2018 and refined by full-matrix least-squares techniques using the SHELXL-2018 software package incorporated in WinGX system version v2018.3. For molecular-level DFT calculations, the Gaussian 09 D.01program was used. Powder X-ray diffraction data of microcrystalline powders was collected using a D8 Advance Bruker instrument with Cu Kα Xray source 1.54 Å. An optical microscope of LEICA equipped with LAS V4.8 software was used to see the single crystals of NCs at different magnifications and polarization angles. Point EDAX analysis of single crystals was performed with a Verios G4 UC FEI instrument. Crystals were drop-cast onto the substrate (TEM grid) and dried at room temperature. The sample was sputter-coated with gold (Au) for better-quality images. Aliquot was drop casted on the substrate (TEM grid, glow discharged) and dried at room temperature. For Transmission electron microscopy (TEM), the Talos F200i instrument operated at 200 kV was used.

Computational details

Molecular DFT calculations were performed with Gaussian 09 D.01.[2] In all calculations, real ligand without modification was considered. Geometry optimizations and harmonic vibrational frequency analyses were carried out at the B3LYP level, which combines Becke's three-parameter hybrid exchange functional with the Lee–Yang–Parr correlation functional. Empirical dispersion effects were included via Grimme's D3 correction. Non-metal atoms (C, H, P, S, F) were described by Pople's split-valence 6-31G(d,p) basis set, while silver atoms were treated with the LANL2DZ effective core potential and its accompanying double-ζ valence basis.[3-10] Solvent effects (methanol) were modeled using the conductor-like polarizable continuum model (CPCM).

Time-dependent DFT calculations were carried out at the PBE level of theory. Self-consistent-field (SCF) convergence was achieved with a maximum of 1,000 cycles. Excited states were computed using the linear-response formalism, with 500 singlet-to-singlet transitions requested and an energy damping threshold (DEMin) of 2,000 cm^{-1} to improve root-finding stability. Kohn–Sham orbital contributions to each excitation were analyzed using Multiwfn 3.6.[11] enabling visualization of frontier-orbital character and charge-transfer pathways.

Periodic boundary–condition calculations were carried out using the Vienna Ab Initio Simulation Package (VASP),[12–14] employing the Perdew–Burke–Ernzerhof (PBE) generalized gradient approximation for exchange–correlation. Ion–electron interactions were treated via the projector augmented-wave (PAW) method.[15,16] Ionic relaxations were performed with a conjugate-gradient algorithm, enforcing an energy convergence of 10^{-4} eV and a Hellmann–Feynman force threshold of 0.02 eV $Å^{-1}$. Given the large unit-cell sizes, Brillouin-zone sampling was restricted to the Γ-point (1×1×1). For density of states (DOS) analyses, a denser 3×3×3 k-point mesh was used.

Table 1. Crystal data and structure refinement for Ag-1.

Identification code	shelx	
Empirical formula	$C_{61}H_{45}AgF_7P_3S$	
Formula weight	1143.81	
Temperature	143(2) K	
Wavelength	0.71073 Å	
Crystal system	Triclinic	
Space group	P-1	
Unit cell dimensions	a = 12.5786(9) Å	a= 87.211(3)°.
	b = 12.8514(10) Å	b= 85.428(3)°.
	c = 16.1604(14) Å	g = 82.345(3)°.
Volume	2578.9(4) $Å^3$	
Z	2	
Density (calculated)	1.473 Mg/m^3	
Absorption coefficient	0.590 mm^{-1}	
F(000)	1164	
Crystal size	0.237 x 0.125 x 0.112 mm^3	
Theta range for data collection	3.046 to 24.999°.	
Index ranges	-14<=h<=14, -15<=k<=15, -19<=l<=19	
Reflections collected	74543	

Independent reflections	9059 [R(int) = 0.0343]
Completeness to theta = 24.999°	99.8 %
Absorption correction	Semi-empirical from equivalents
Max. and min. transmission	0.7457 and 0.6966
Refinement method	Full-matrix least-squares on F^2
Data / restraints / parameters	9059 / 2 / 658
Goodness-of-fit on F^2	1.057
Final R indices [I>2sigma(I)]	R1 = 0.0318, wR2 = 0.0825
R indices (all data)	R1 = 0.0358, wR2 = 0.0862
Extinction coefficient	n/a
Largest diff. peak and hole	1.988 and -0.893 e.Å^{-3}

Table 2. Atomic coordinates (x 10^4) and equivalent isotropic displacement parameters (Å^{2}x 10^3)
for Ag-1. U(eq) is defined as one third of the trace of the orthogonalized U^{ij} tensor.

	x	y	z	U(eq)
Ag(1)	7559(1)	7257(1)	2504(1)	18(1)
C(1)	7244(2)	9123(2)	4196(2)	20(1)
C(2)	7990(2)	9694(3)	3758(2)	32(1)
C(3)	8577(3)	10322(3)	4167(2)	39(1)
C(4)	8442(2)	10367(3)	5025(2)	35(1)
C(5)	7704(2)	9804(3)	5463(2)	34(1)
C(6)	7106(2)	9185(2)	5054(2)	26(1)
C(7)	6172(2)	6696(2)	4686(2)	33(1)
C(8)	5693(2)	7664(2)	4397(2)	19(1)
C(9)	4665(2)	8046(2)	4722(2)	23(1)
C(10)	4132(2)	7464(2)	5331(2)	30(1)
C(11)	4625(3)	6513(3)	5626(2)	37(1)
C(12)	5646(3)	6129(3)	5306(2)	44(1)
C(13)	5436(2)	9376(2)	3204(2)	18(1)
C(14)	5359(2)	10443(2)	3366(2)	24(1)
C(15)	4569(2)	11160(2)	3034(2)	30(1)
C(16)	3840(2)	10826(2)	2540(2)	31(1)
C(17)	3904(2)	9770(2)	2378(2)	30(1)

C(18)	4699(2)	9051(2)	2703(2)	24(1)
C(19)	9491(2)	9184(2)	1829(2)	18(1)
C(20)	9408(2)	10263(2)	1655(2)	22(1)
C(21)	10079(2)	10869(2)	2010(2)	27(1)
C(22)	10842(2)	10403(2)	2525(2)	28(1)
C(23)	10934(2)	9327(2)	2701(2)	28(1)
C(24)	10258(2)	8721(2)	2361(2)	23(1)
C(25)	9545(2)	7604(2)	633(2)	21(1)
C(26)	10561(2)	7868(2)	382(2)	28(1)
C(27)	11189(2)	7327(3)	-245(2)	37(1)
C(28)	10810(3)	6541(3)	-634(2)	42(1)
C(29)	9801(3)	6275(3)	-393(2)	51(1)
C(30)	9178(2)	6798(3)	245(2)	41(1)
C(31)	7799(2)	9268(2)	758(2)	17(1)
C(32)	8131(2)	9579(2)	-47(2)	23(1)
C(33)	7483(2)	10325(2)	-492(2)	29(1)
C(34)	6491(2)	10759(2)	-144(2)	31(1)
C(35)	6151(2)	10454(2)	654(2)	29(1)
C(36)	6800(2)	9713(2)	1103(2)	22(1)
C(37)	6456(2)	6251(2)	709(2)	20(1)
C(38)	6259(2)	7282(2)	390(2)	23(1)
C(39)	6377(2)	7506(2)	-459(2)	29(1)
C(40)	6700(2)	6703(3)	-999(2)	33(1)
C(41)	6901(3)	5679(3)	-690(2)	35(1)
C(42)	6782(2)	5451(2)	160(2)	26(1)
C(43)	6635(2)	4659(2)	2055(2)	20(1)
C(44)	5978(2)	3975(2)	1768(2)	27(1)
C(45)	6198(2)	2903(2)	1934(2)	32(1)
C(46)	7054(3)	2505(2)	2393(2)	34(1)
C(47)	7696(2)	3176(2)	2691(2)	30(1)
C(48)	7489(2)	4258(2)	2520(2)	23(1)
C(49)	4924(2)	6327(2)	2124(2)	20(1)
C(50)	4146(2)	6633(2)	1561(2)	25(1)
C(51)	3066(2)	6838(2)	1845(2)	32(1)
C(52)	2753(2)	6737(2)	2680(2)	31(1)
C(53)	3521(2)	6435(2)	3243(2)	29(1)
C(54)	4598(2)	6231(2)	2966(2)	24(1)
C(55)	9191(2)	6232(2)	4146(2)	30(1)

C(56)	8727(2)	5477(2)	4660(2)	31(1)
C(57)	8621(2)	5499(2)	5515(2)	33(1)
C(58)	8980(2)	6287(2)	5932(2)	34(1)
C(59)	9473(3)	7026(2)	5433(2)	37(1)
C(60)	9581(3)	6997(2)	4587(2)	35(1)
C(61)	8785(3)	6428(3)	6845(2)	40(1)
F(1)	9856(2)	7806(2)	5799(1)	55(1)
F(2)	10084(2)	7741(2)	4167(1)	53(1)
F(3)	8332(2)	4687(2)	4311(1)	45(1)
F(4)	8141(2)	4741(2)	5924(1)	49(1)
F(5)	8364(2)	5646(2)	7259(1)	55(1)
F(6)	8117(2)	7306(2)	7003(1)	62(1)
F(7)	9696(2)	6536(2)	7207(1)	58(1)
P(1)	6460(1)	8372(1)	3599(1)	17(1)
P(2)	8625(1)	8332(1)	1405(1)	16(1)
P(3)	6376(1)	6077(1)	1843(1)	18(1)
S(1)	9283(1)	6202(1)	3077(1)	31(1)

Table 3. Crystal data and structure refinement for Ag-6.

Identification code	shelx	
Empirical formula	$C_{150} H_{90} Ag_6 F_{42} P_6 S_6$	
Formula weight	3715.61	
Temperature	298(2) K	
Wavelength	0.71073 Å	
Crystal system	Trigonal	
Space group	R -3:H	
Unit cell dimensions	a = 29.0591(12) Å	a= 90°.
	b = 29.0591(12) Å	b= 90°.
	c = 14.8748(9) Å	g = 120°.
Volume	10877.9(11) Å^3	
Z	3	
Density (calculated)	1.702 Mg/m^3	
Absorption coefficient	1.052 mm^{-1}	
F(000)	5508	
Crystal size	0.123 x 0.095 x 0.082 mm^3	

Theta range for data collection	2.542 to 24.987°.
Index ranges	-34<=h<=34, -34<=k<=34, -16<=l<=17
Reflections collected	38105
Independent reflections	4248 [R(int) = 0.1031]
Completeness to theta = 24.987°	99.8 %
Absorption correction	Semi-empirical from equivalents
Max. and min. transmission	0.7457 and 0.6647
Refinement method	Full-matrix least-squares on F^2
Data / restraints / parameters	4248 / 129 / 344
Goodness-of-fit on F^2	1.146
Final R indices [I>2sigma(I)]	R1 = 0.0979, wR2 = 0.1899
R indices (all data)	R1 = 0.1280, wR2 = 0.2079
Extinction coefficient	n/a
Largest diff. peak and hole	0.786 and -1.693 e.Å^{-3}

Table 4. Atomic coordinates (x 10^4) and equivalent isotropic displacement parameters (Å^{2}x 10^3)
for Ag-6 . U(eq) is defined as one third of the trace of the orthogonalized U^{ij} tensor.

	x	y	z	U(eq)
Ag(1)	3153(1)	5631(1)	2586(1)	40(1)
S(1)	2414(1)	5896(1)	2554(2)	30(1)
P(1)	3102(1)	4949(1)	3591(2)	29(1)
C(1)	3354(4)	4531(4)	3126(8)	39(3)
C(2)	3180(5)	4019(4)	3405(8)	48(3)
C(3)	3407(6)	3731(6)	3083(11)	72(4)
C(4)	3815(6)	3974(7)	2481(11)	74(4)
C(5)	3995(7)	4477(8)	2188(10)	82(5)
C(6)	3758(5)	4753(5)	2490(9)	59(3)
C(7)	3484(4)	5223(4)	4625(7)	34(2)
C(8)	3733(5)	4992(5)	5083(9)	63(4)
C(9)	3989(7)	5217(8)	5891(12)	98(6)
C(10)	3971(7)	5627(7)	6251(10)	79(5)
C(11)	3742(5)	5870(6)	5832(9)	62(4)

C(12)	3488(5)	5662(5)	5017(9)	56(3)
C(13)	2432(4)	4459(4)	3990(7)	28(2)
C(14)	2320(4)	4255(4)	4839(8)	46(3)
C(15)	1806(5)	3873(5)	5082(9)	58(4)
C(16)	1411(5)	3704(6)	4493(11)	67(4)
C(17)	1500(5)	3907(6)	3620(11)	68(4)
C(18)	2015(4)	4281(5)	3378(9)	53(3)
C(19)	1868(4)	5466(4)	3221(7)	34(2)
C(20)	1912(4)	5353(4)	4107(8)	38(3)
C(21)	1482(5)	5029(5)	4645(7)	47(3)
C(22)	978(5)	4793(5)	4325(9)	49(3)
C(23)	923(4)	4879(5)	3433(10)	54(3)
C(24)	1335(4)	5199(4)	2898(8)	36(3)
F(1)	2397(2)	5578(3)	4479(4)	51(2)
F(2)	1585(3)	4959(3)	5494(5)	74(2)
F(3)	430(3)	4645(4)	3061(7)	101(3)
F(4)	1242(3)	5260(3)	2035(5)	64(2)
C(25)	515(5)	4456(6)	4921(11)	87(5)
F(5)	450(15)	4703(11)	5590(20)	132(13)
F(6)	552(10)	4056(10)	5260(20)	118(10)
F(7)	60(7)	4185(13)	4490(20)	127(12)
F(5')	223(19)	3975(11)	4640(30)	147(17)
F(6')	188(12)	4645(14)	4910(30)	123(12)
F(7')	628(15)	4500(20)	5781(14)	143(17)

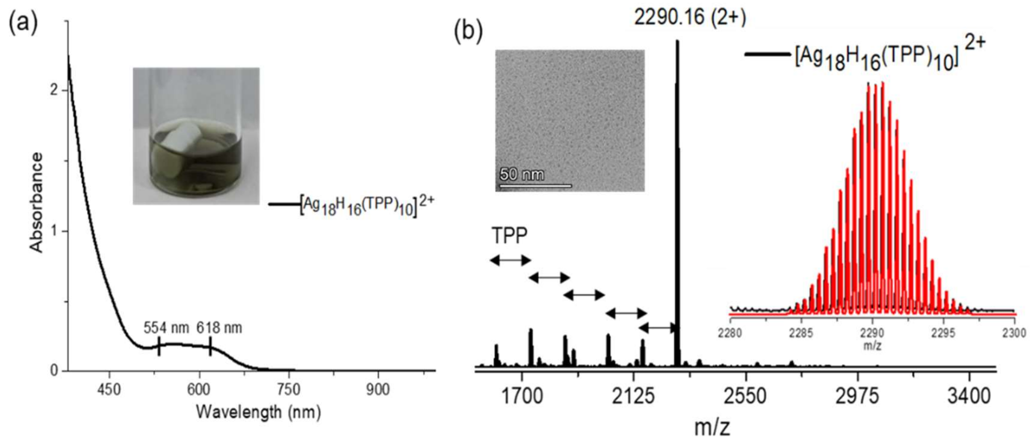

Fig. S1 (a) UV-vis spectrum (inset shows photograph of Ag_{18} NC in methanol). (b) ESI-MS spectrum of Ag_{18} NC and exact matching of the experimental spectrum (black) and simulated spectrum (red). Peaks below m/z 2290.16 are due to loss of triphenyl phosphines (marked with arrow).Inset shows TEM image of Ag_{18} NC.

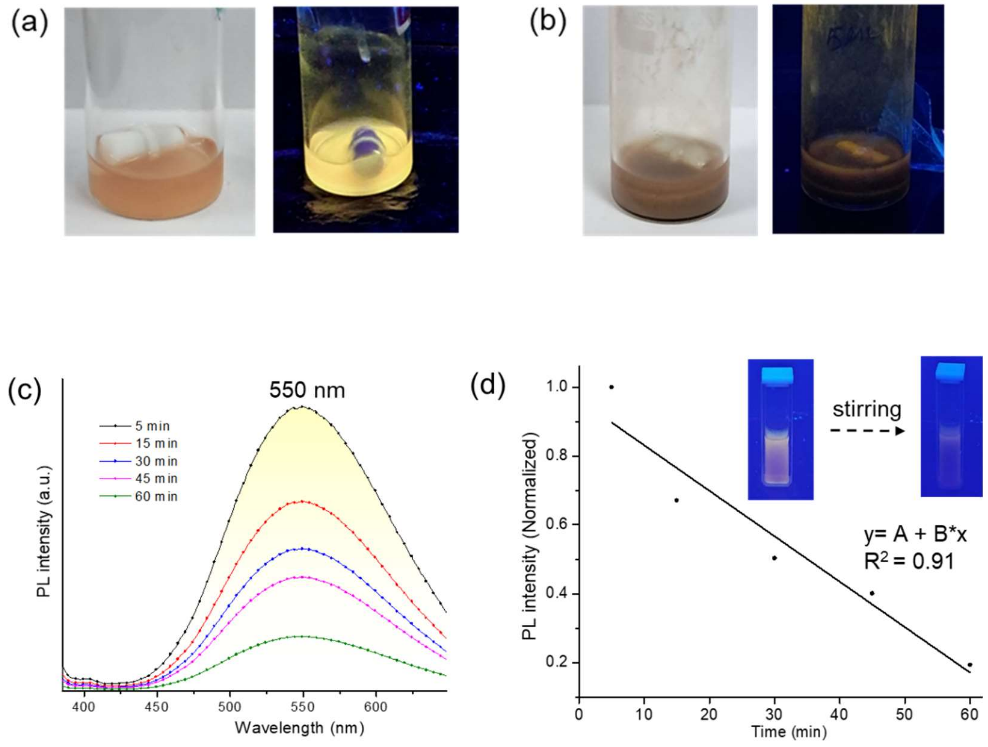

Fig. S2 Reaction mixture for the cluster and thiol ratio of 1:1. Solution under visible (left side photos) and uv light (right side photos) after (a) 5 min and (b) 45 min of reaction. (c) Time dependent PL spectra of LEIST showing quenched emission with progress of the reaction. (d) Spectrum between normalized PL intensity and reaction time suggests decrease of photoluminescence with progress of reaction, inset photographs show quenched emission upon stirring.

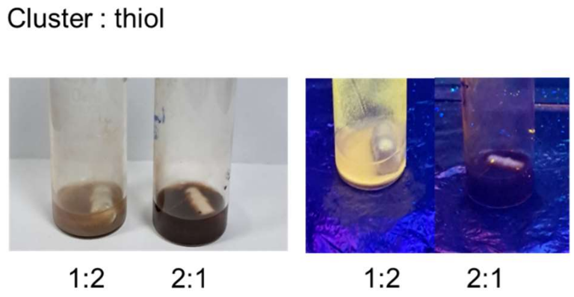

Fig. S3 Photograph of reaction mixture (cluster and thiol ratios of 1:2 and 2:1, respectively) under visible (left) and uv (right) light. Reaction mixture of 1:2 always retains yellow emission upon stirring even after 60 min, whereas for 2:1 reaction no emission was observed.

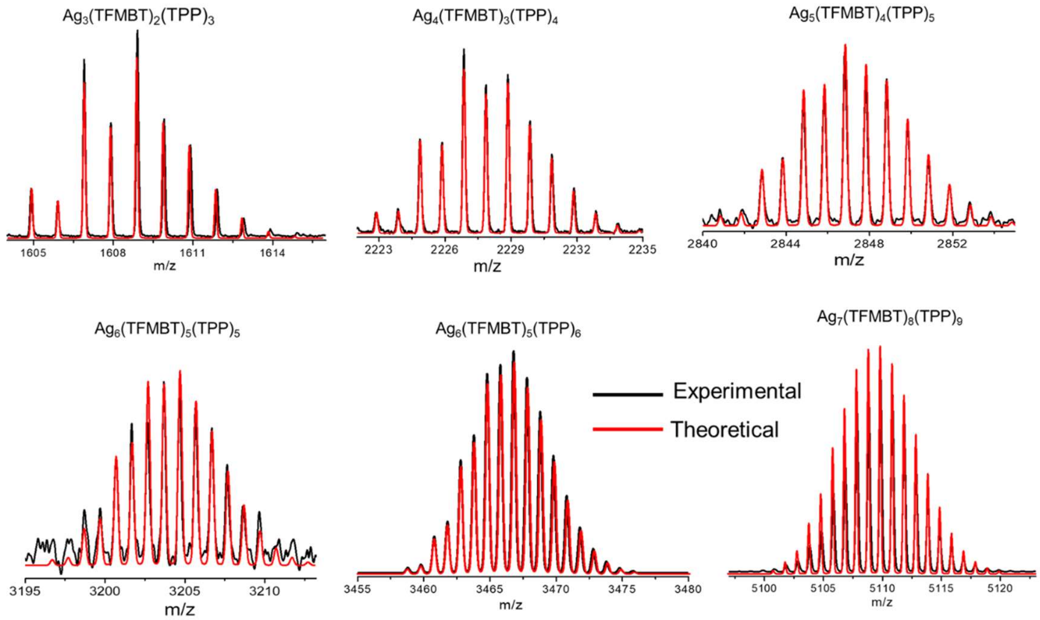

Fig. S4 Matching between the isotopic mass distributions of the experimental and simulated spectra.

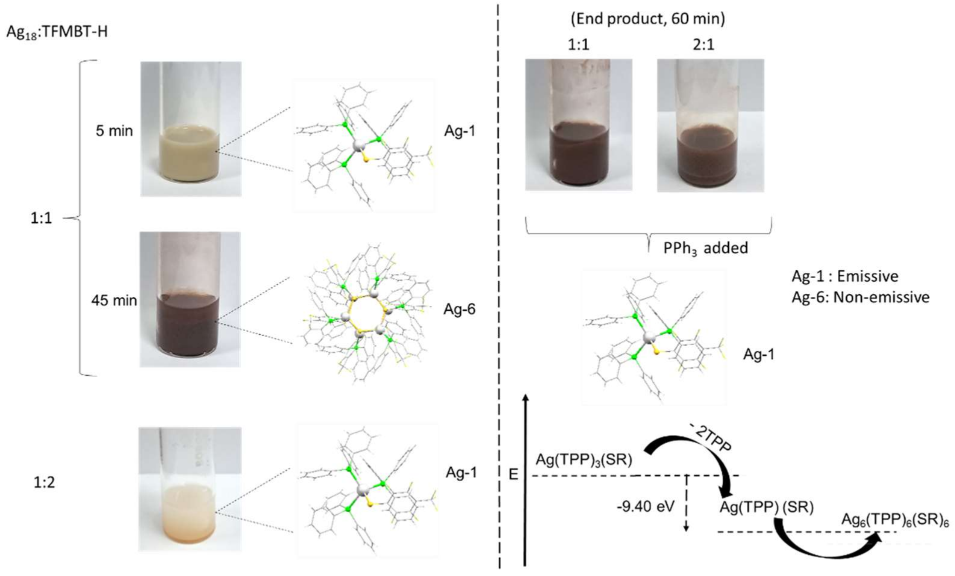

Fig. S5 Scheme describes crystallization steps of Ag-1 and Ag-6. Theoretical approach shows energetically favourable path from Ag-1 to Ag-6.

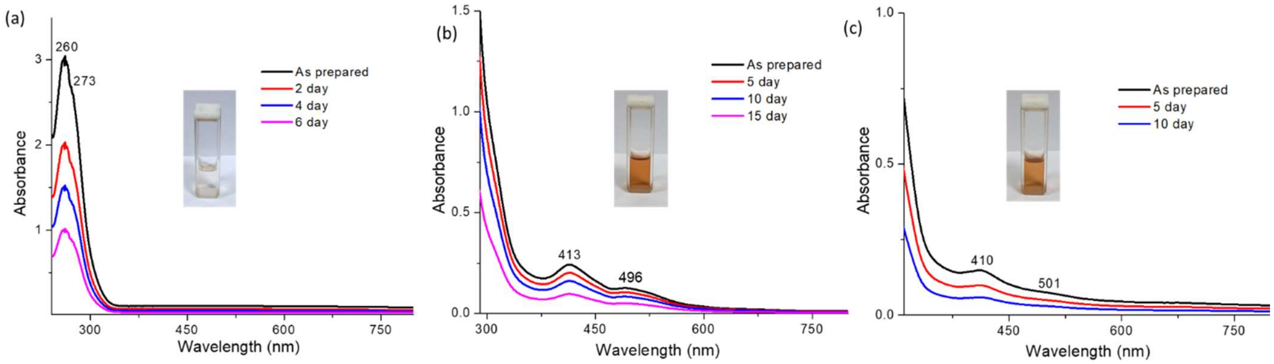

Fig. S6 Stability check through UV-vis study in methanol. UV-vis spectra of (a) Ag-1, (b) Ag-6, and (c) Ag-7 show time-dependent stability. Insets show the photographs of the respective solutions.

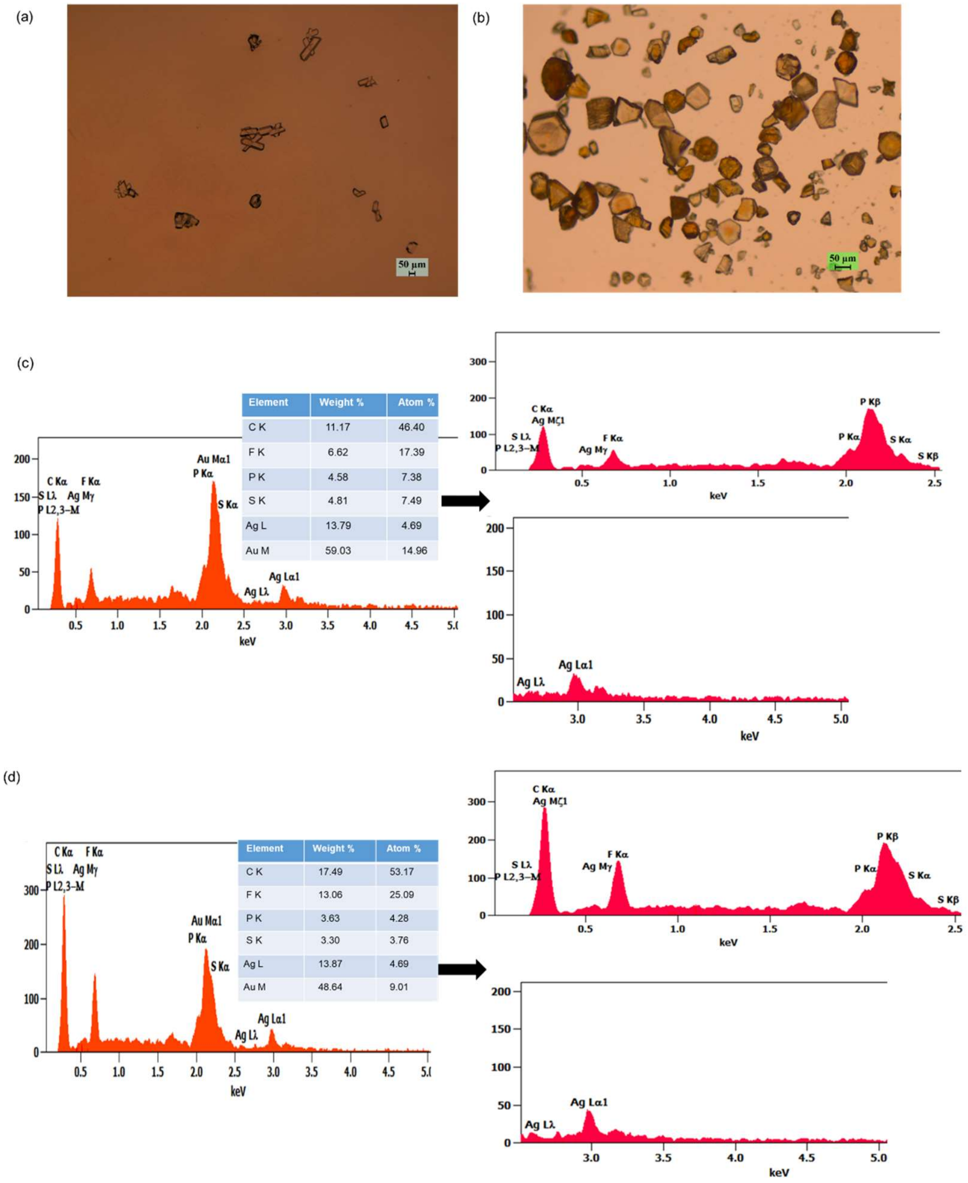

Element	Weight %	Atom %
C K	11.17	46.40
F K	6.62	17.39
P K	4.58	7.38
S K	4.81	7.49
Ag L	13.79	4.69
Au M	59.03	14.96

Element	Weight %	Atom %
C K	17.49	53.17
F K	13.06	25.09
P K	3.63	4.28
S K	3.30	3.76
Ag L	13.87	4.69
Au M	48.64	9.01

Fig. S7 Optical images of (a) Ag-1 and (b) Ag-6. (c,d) point EDAX spectra of Ag-1 and Ag-6, respectively. Inset tables show weight% and atom % of elements. Zoomed-in views of the respective spectra show the presence of different elements. Au peak was observed due to sputtering of the sample before doing SEM.

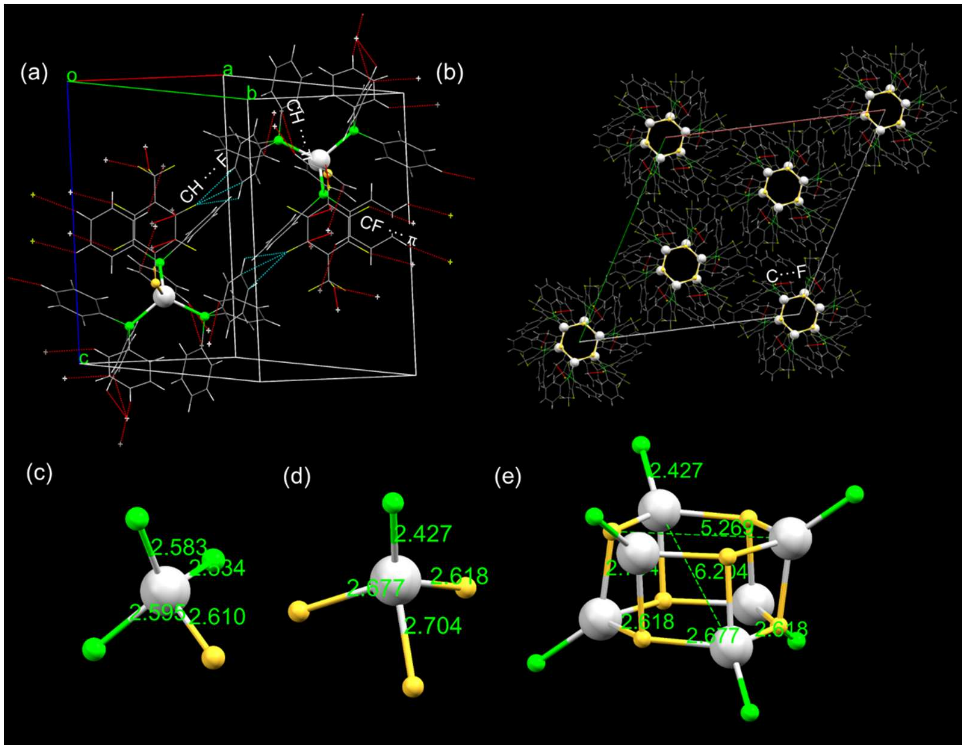

Fig. S8 (a) Two Ag-1 and (b) three Ag-6 per unit cell. (c, d) Ag-S and Ag-P bond distances in Ag-1 and Ag-6, respectively. (e) Ag-Ag and Ag-S distances in Ag_6S_6 rigid frame.

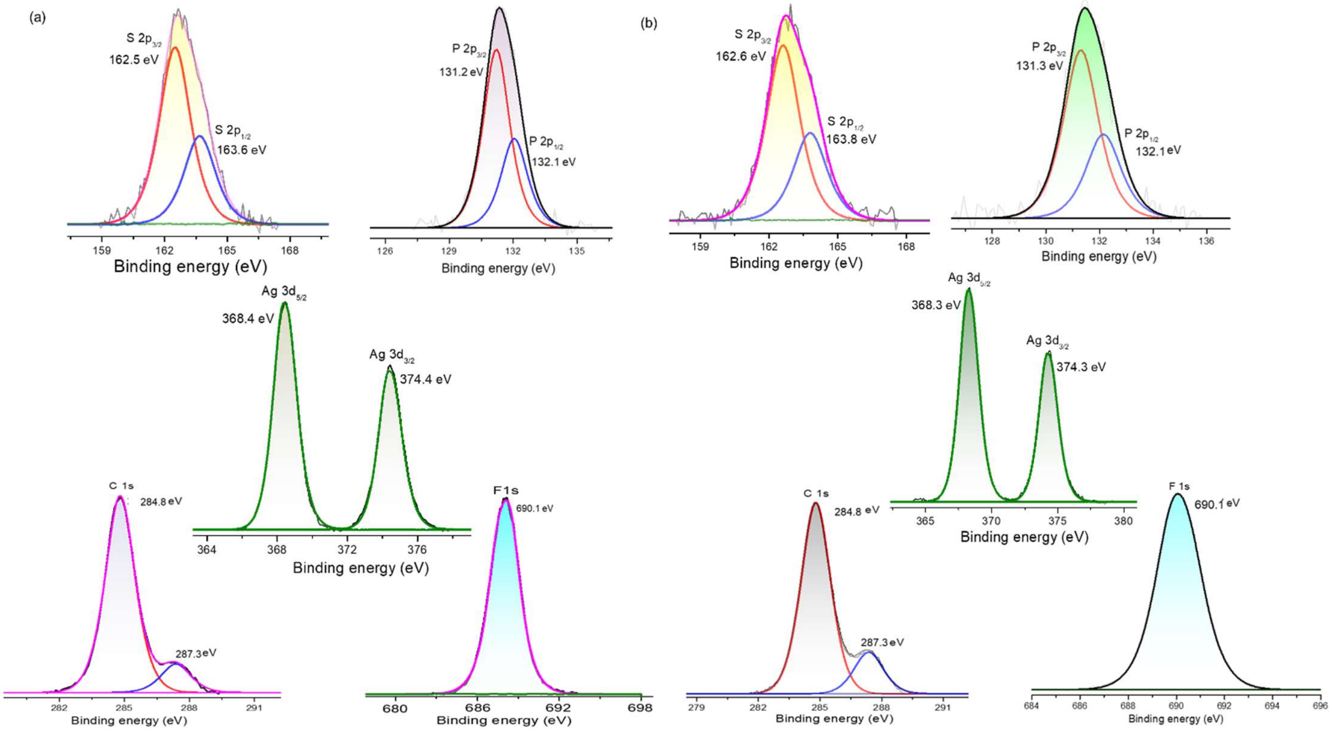

Fig. S9 XPS spectra of respective element in (a) Ag-1 and (b) Ag-6, respectively.

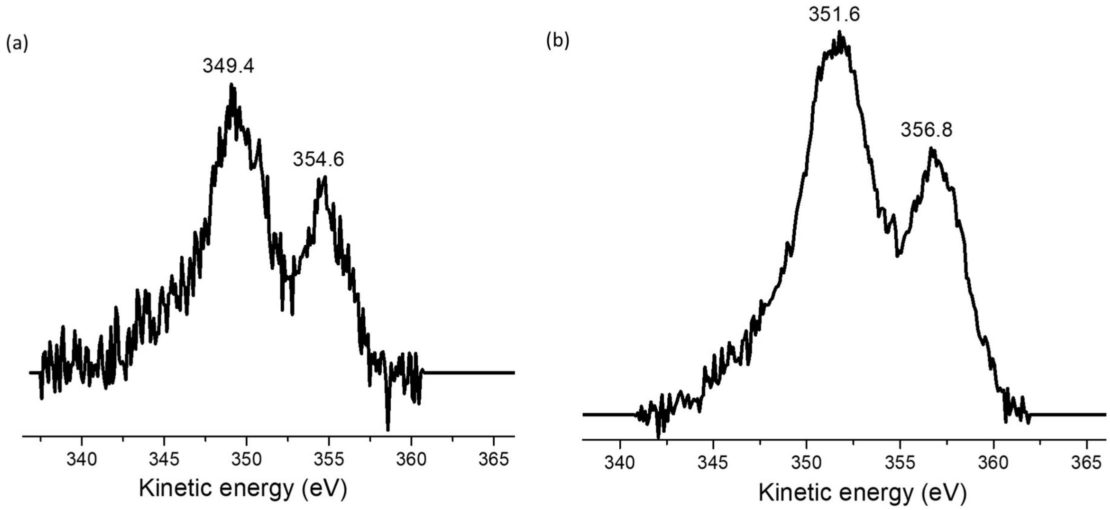

Fig. S10 Ag MNN Auger spectra of (a) Ag-1 and (b) Ag-6, respectively.

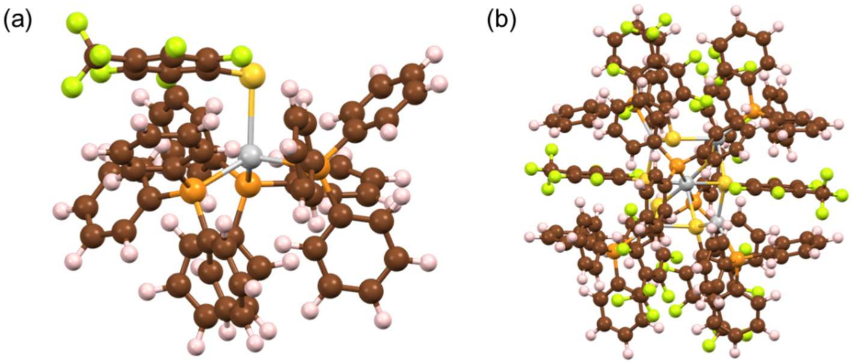

Fig. S11 DFT optimized structure of (a) Ag-1 and (b) Ag-6. Real ligands (phosphine and thiol) were considered in calculation.

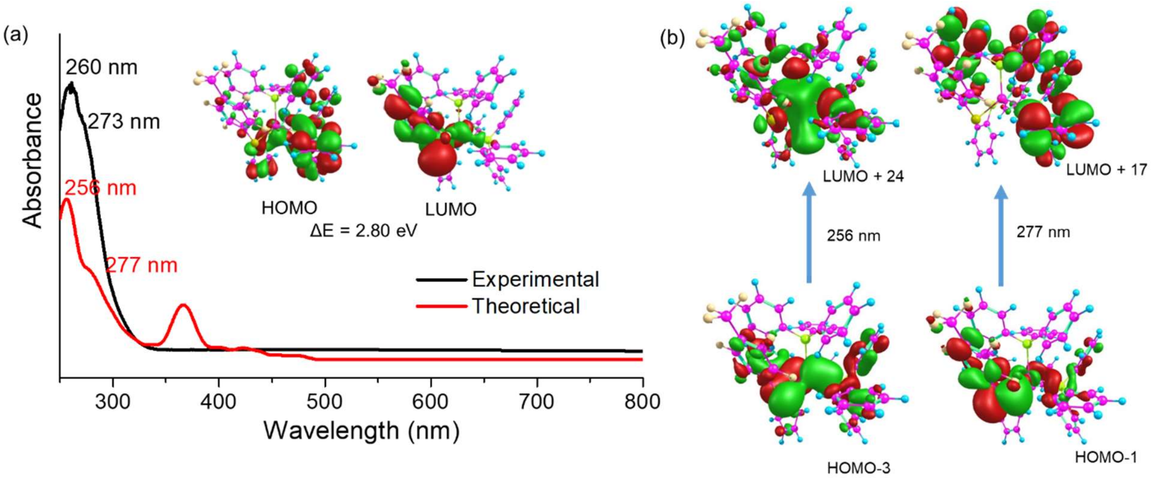

Fig. S12 (a) Experimental and theoretical UV-vis spectra of Ag-1 (inset images are HOMO and LUMO). (b) Electronic transitions involving molecular orbitals.

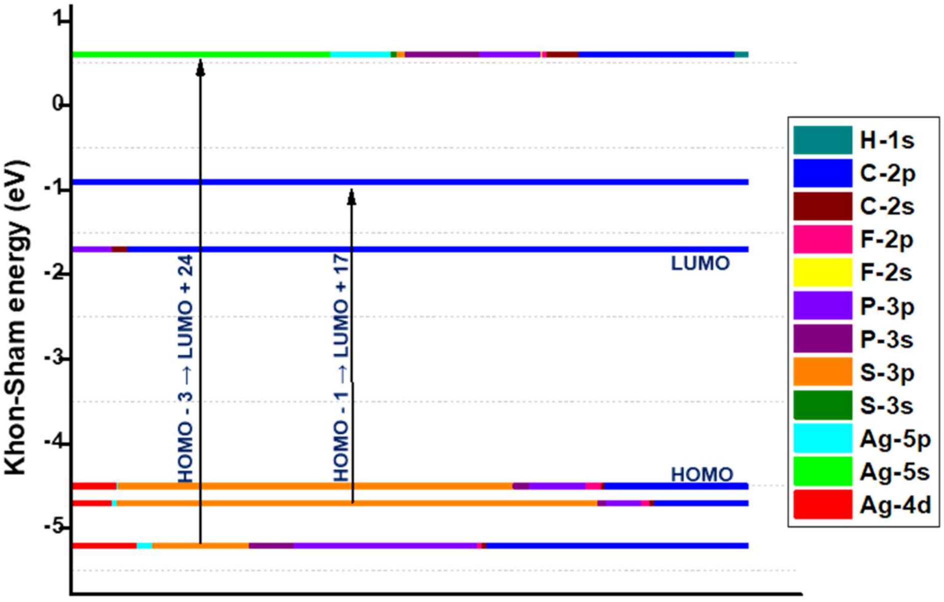

Fig. S13 The Kohn-Sham (K-S) molecular orbital (MO) analysis for Ag-1.

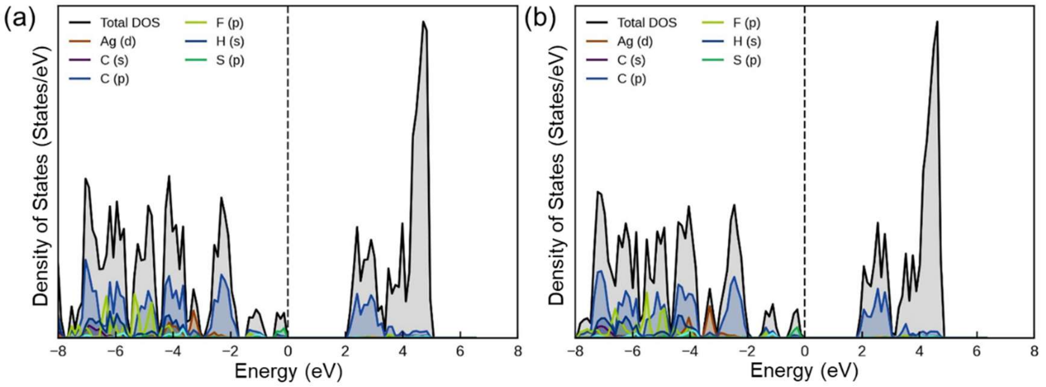

Fig. S14 Projected density of states for (a) SC-XRD and (b) DFT optimized structure of Ag-1. The respective band gaps are 2.80 and 2.30 eV, respectively.

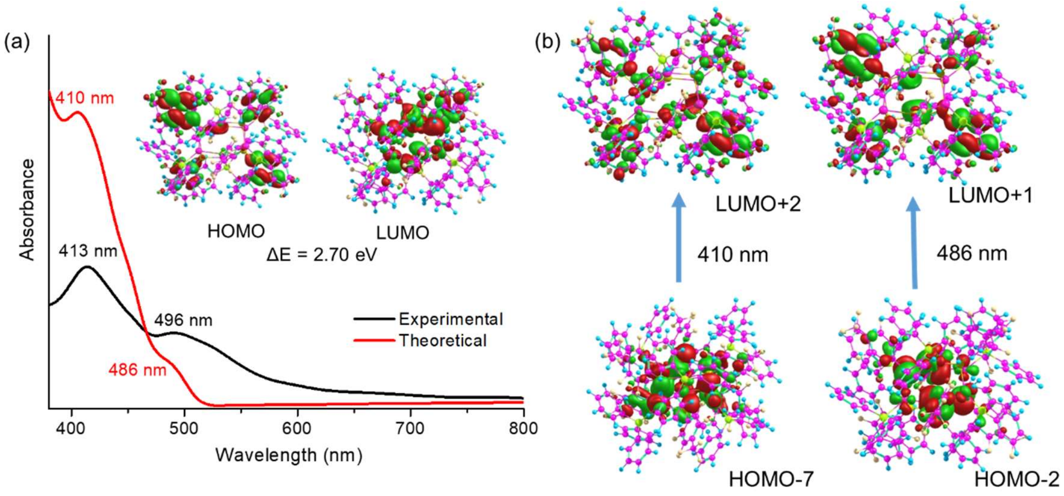

Fig. S15 (a) Experimental and theoretical UV-vis spectra of Ag-6 (inset images are HOMO and LUMO). (b) Electronic transitions involving molecular orbitals.

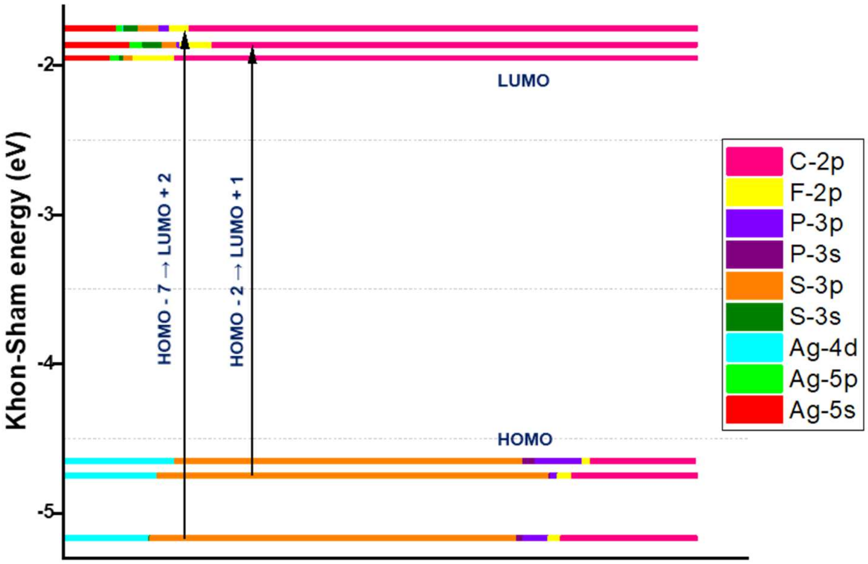

Fig. S16 The Kohn-Sham (K-S) molecular orbital (MO) analysis for Ag-6.

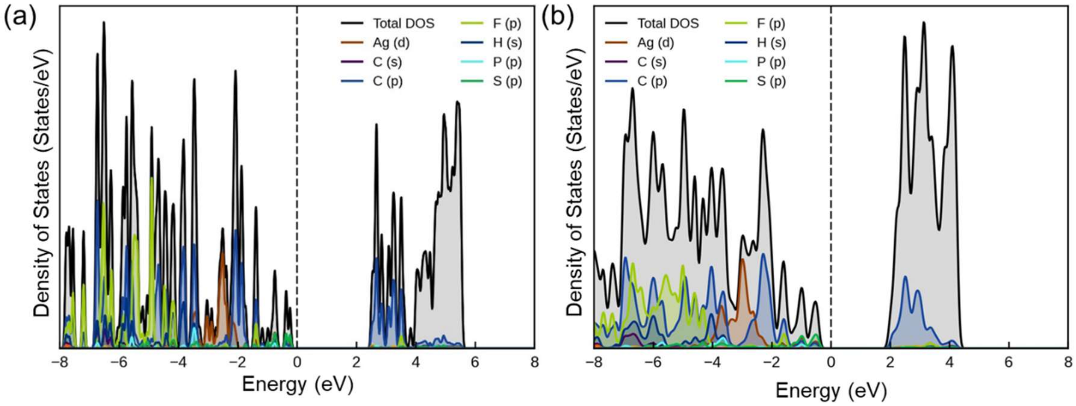

Fig. S17 Projected density of states for (a) SC-XRD and (b) DFT optimized structure of Ag-6. Respective band gaps are 2.70 and 2.50 eV, respectively.

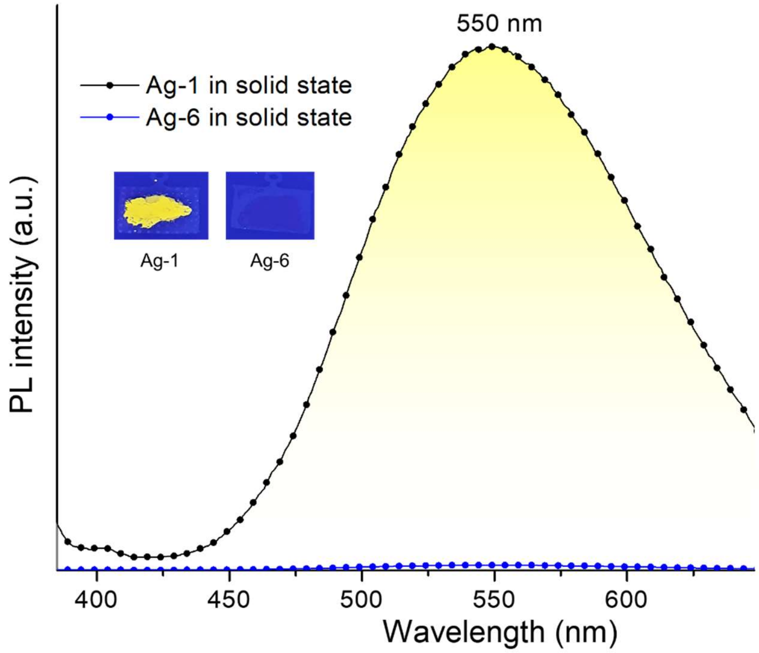

Fig. S18 Emission spectra of Ag-1 and Ag-6 in solid state (excitation at 365 nm).

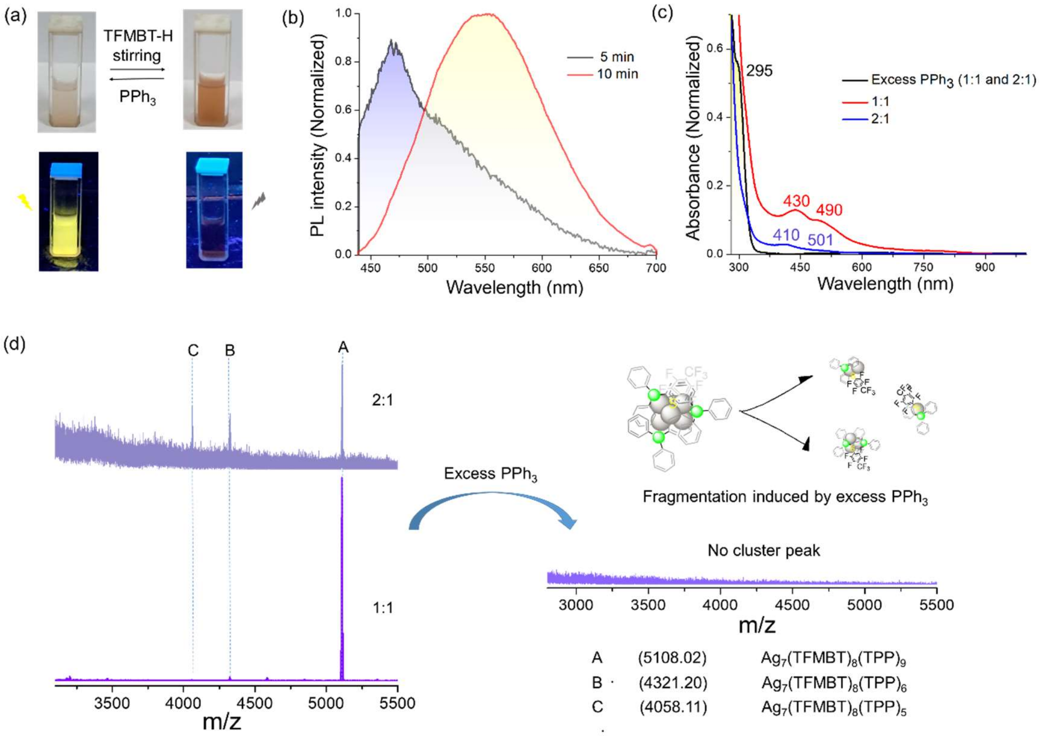

Fig. S19 (a) Photograph of PPh$_3$- induced switching of the reaction (cluster to thiol ratio of 1:1). (b,c) Normalized PL spectra recorded at 5 and 10 min respectively showing emergence of yellow emission, and changes in UV-vis spectra in presence of externally added PPh$_3$. (d) ESI MS spectra reveal the fragmentation of larger cluster core induced by PPh$_3$.

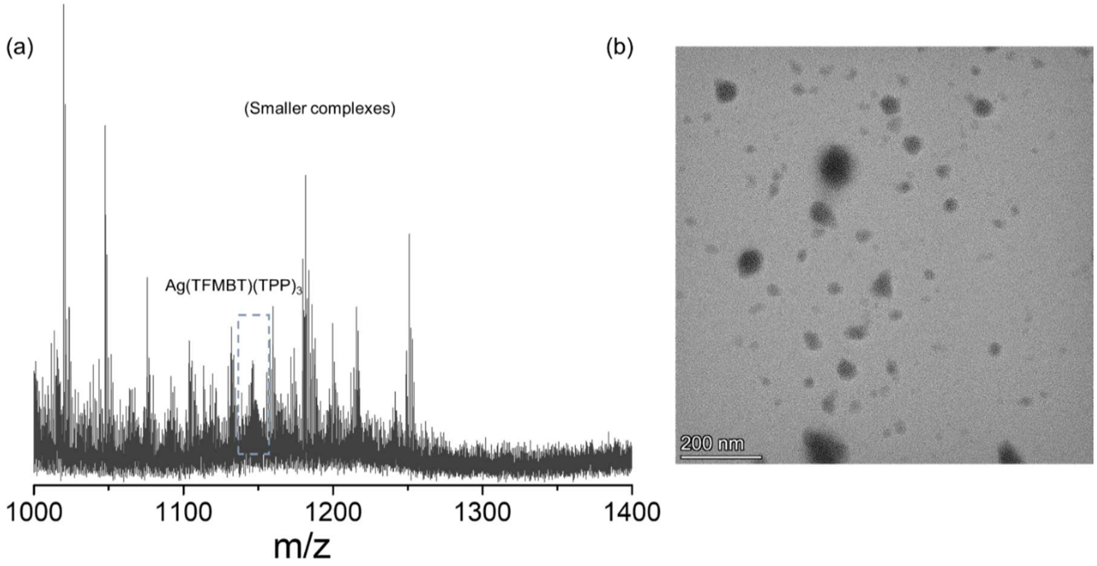

Fig. S20 (a) ESI MS spectra reveal small complexes due to addition of excess PPh_3 to end product mixture of cluster to thiol ratios of 1:1 and 2:1. (b) TEM image show aggregates.

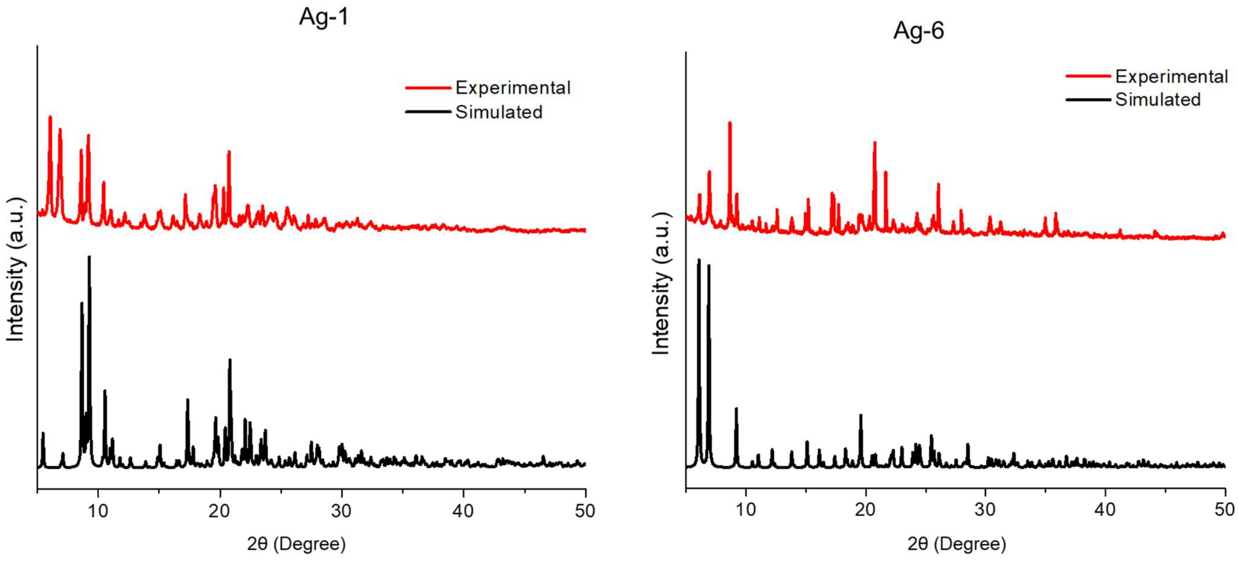

Fig. S21 Comparative powder X-ray diffraction pattern of (a) Ag-1 and (b) Ag-6.

References

1 M.S. Bootharaju, R. Dey, L.E. Gevers, M.N. Hedhili, J.M. Basset and O.M. Bakr, *J. Am. Chem. Soc.* 2016, **138**, 13770-13773.

2 Gaussian 09, Revision D.01, M.J. Frisch, G.W. Trucks, H.B. Schlegel, G.E. Scuseria, M.A.Robb, J.R. Cheeseman, G. Scalmani, V. Barone, B. Mennucci, G.A. Petersson, H. Nakatsuji, M. Caricato, X. Li, H.P. Hratchian, A.F. Izmaylov, J. Bloino, G. Zheng, J.L. Sonnenberg, M. Hada, M. Ehara, K. Toyota, R. Fukuda, J. Hasegawa, M. Ishida, T. Nakajima, Y. Honda, O. Kitao, H. Nakai, T. Vreven, J.A. Montgomery, Jr., J.E. Peralta, F. Ogliaro, M. Bearpark, J.J. Heyd, E. Brothers, K.N. Kudin, V.N. Staroverov, T. Keith, R. Kobayashi, J. Normand, K. Raghavachari, A. Rendell, J.C. Burant, S.S. Iyengar, J. Tomasi, M. Cossi, N. Rega, J.M. Millam, M. Klene, J.E. Knox, J.B. Cross, V. Bakken, C. Adamo, J. Jaramillo, R. Gomperts, R.E. Stratmann, O. Yazyev, A.J. Austin, R. Cammi, C. Pomelli, J.W. Ochterski, R.L. Martin, K. Morokuma, V.G. Zakrzewski, G.A. Voth, P. Salvador, J.J. Dannenberg, S. Dapprich, A.D. Daniels, O. Farkas, J.B. Foresman, J.V. Ortiz, J. Cioslowski and D.J. Fox, Gaussian, Inc., Wallingford CT 2013.

3 A.D. Becke, *J. Chem. Phys.* 1993, **98**, 5648−5652.

4 A.D. Becke, *J. Chem. Phys.* 1996, **104**, 1040−1046.

5 C.T. Lee, W.T. Yang and R.G. Parr, *Phys. Rev. B: Condens. Matter Mater. Phys.* 1988, **37**, 785−789.

6 T. Clark, J. Chandrasekhar, G.W. Spitznagel and P. Schleyer, *J. Comput. Chem.* 1983, **4**, 294−301.

7 P.C. Hariharan and J.A. Pople, *Theor. Chim. Acta* 1973, **28**, 213−222.

8 P.J. Hay and W.R. Wadt, *J. Chem. Phys.* 1985, **82**, 270−283.

9 S. Grimme, J. Antony, S. Ehrlich and H. Krieg, *J. Chem. Phys.* 2010, **132**, 154104.

10 T. Lu and F. Chen, *J. Comput. Chem.* 2012, **33**, 580-592.

11 G. Kresse and J. Furthmüller, Comput. *Mater. Sci.* 1996, **6**, 15−50.

12 J.P. Perdew, K. Burke and M. Ernzerhof, *Phys. Rev. Lett.* 1996, **77**, 3865-3868.

13 J.P. Perdew, K. Burke and M. Ernzerhof, *Phys. Rev. Lett.* 1997, **78**, 1396−1396.

14 P.E. Blöchl, *Phys. Rev. B: Condens. Matter Mater. Phys.* 1994, **50**, 17953−17979.

15 G. Kresse and D. Joubert, *Phys. Rev. B: Condens. Matter Mater. Phys.* 1999, **59**, 1758−1775.

16 G. Kresse and J. Furthmuller, *Phys.Rev.B: Condens.Matter.Phys.* 1996, **51**, 11169-11186.